ACS APPLIED MATERIALS & INTERFACES

Research Article

www.acsami.org

Ceramic Barrier Layers for Flexible Thin Film Solar Cells on Metallic Substrates: A Laboratory Scale Study for Process Optimization and Barrier Layer Properties

Jose-Maria Delgado-Sanchez,*[,†] Nuria Guilera,[‡] Laia Francesch,[‡] Maria D. Alba,*[,§] Laura Lopez,[‡] and Emilio Sanchez[†]

[†]Abengoa Solar New Technologies S.A., Soland Center, Ctra. A472 km 6, 41800 Sanlucar la Mayor, Sevilla, Spain

[‡]CETEMMSA Technological Centre, Av. Ernest Lluch 36, E-08302 Mataró, Spain

[§]Instituto Ciencia de los Materiales de Sevilla (CSIC-US). Avda. Americo Vespucio, 49 , 41008 Sevilla, Spain

ABSTRACT: Flexible thin film solar cells are an alternative to both utility-scale and building integrated photovoltaic installations. The fabrication of these devices over electrically conducting low-cost foils requires the deposition of dielectric barrier layers to flatten the substrate surface, provide electrical isolation between the substrate and the device, and avoid the diffusion of metal impurities during the relatively high temperatures required to deposit the rest of the solar cell device layers. The typical roughness of low-cost stainless-steel foils is in the hundred-nanometer range, which is comparable or larger than the thin film layers comprising the device and this may result in electrical shunts that decrease solar cell performance. This manuscript assesses the properties of different single-layer and bilayer structures containing ceramics inks formulations based on Al_2O_3, AlN, or Si_3N_4 nanoparticles and deposited over stainless-steel foils using a rotogravure printing process. The best control of the substrate roughness was achieved for bilayers of Al_2O_3 or AlN with mixed particle size, which reduced the roughness and prevented the diffusion of metals impurities but AlN bilayers exhibited as well the best electrical insulation properties.

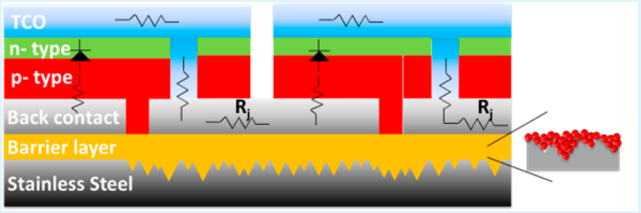

KEYWORDS: *flexible substrate, metallic substrate, barrier layer, thin film solar cells, electric insulator, breakdown voltage*

INTRODUCTION

Photovoltaic devices allow direct conversion of the sunlight into electricity and are among the most promising renewable energy sources to reach comparable prices to fossil-fuel-based sources, particularly for high-radiation regions. This goal has been achieved for wafer-based photovoltaic technologies through the price reductions resulting from a rapid increase in manufacturing capacity. As an alternative, thin film solar cells are predicted to enable even lower prices for similar manufacturing volumes and have therefore attracted considerable attention in recent years.[1] Furthermore, thin film solar cells reported conversion efficiencies are nowadays similar or even higher than those reported for multicrystalline silicon-based solar cells.[2,3] Additionally, thin film cells offer key advantages such as a lower cost rigid substrate such as glass and the possibility of utilizing flexible metallic or polymer-based substrates.

Novel applications for photovoltaics are expected for thin and flexible solar modules, mostly for applications in space, aeronautics, and mobile systems.[4] Significant effort has been devoted to the development of flexible and lightweight thin film modules,[5−7] encouraged by the relatively high small-area cell efficiencies obtained on polymer as well as on metallic substrates. A wide variety of substrates have been investigated,[8−12] with flexible metal foils being attractive because of their thermal stability, vacuum compatibility and resulting device reliability. Stainless steel foils ranks among the most industrially feasible metal foils for photovoltaic devices due to their lower costs and similar thermal expansion coefficient to those of the solar cell device layered sta ck.[9−11]

Recently, high efficiency (18,7%) $Cu(In_{1-x}Ga_x)Se_2$ (CIGS) flexible solar cells on stainless steel substrates[13] have been demonstrated to display relatively high proton and electron radiation stability,[14] low weight and high flexibility.[15] These foils offer the possibility of continuous roll-to-roll fabrication which can allow for lower cost than sequential in-line processing. Additionally, these substrates can withstand temperatures above 600 °C without losing their mechanical properties, which in turn allows deposition of the solar cell absorber layer. On the other hand, the diffusion of stainless steel metal impurities, such as Fe, Ni, and Cr, into the absorbed layer during a high-temperature evaporation process can degrade the cell efficiency,[16] and barriers layers capable of preventing impurity diffusion are therefore of considerable current interest.

Received: May 13, 2014
Accepted: October 9, 2014
Published: October 9, 2014

Overall, the fabrication of monolithically integrated thin film photovoltaic modules on electrically conducting substrates requires the deposition of a dielectric barrier.[4,17,18] These barriers must satisfy requirements such as (a) to provide electrical insulation between the metal substrate and the monolithically interconnected solar cells; (b) to reduce the diffusion of impurities from the metal substrate into the solar cells; (c) to flatten the substrate original roughness; and; (d) to provide an appropriated thermal and mechanical stability during device processing.[4,19] These insulation properties are mainly influenced by the barrier thickness, substrate type and deposition process.[4]

Different top-down deposition approaches for these dielectric barrier layers, such as physical vapor deposition or atomic layer deposition, have been investigated.[20] However, significantly less work has been reported using low-cost sol−gel or printing approaches. Herz et al.[21] explored the suitability of Al_2O_3 dielectric layers deposited by RF magnetron sputtering, as diffusion barriers for three different metal substrates and found that the concentrations of Fe and Cr in the thin film solar cell decreased proportionally with increasing the barrier thickness but were not completely suppressed. Their results suggest an Al_2O_3 barrier thickness of ≥2 μm for Cr steel and ≥1 μm for Kovar substrates. These relatively thick barrier layers render this approach unappealing as the deposition rates for such dielectric layers are typically low.

The present paper describes the preparation of different ink formulations based on Al_2O_3, AlN and Si_3N_4 nanoparticles that were deposited over stainless steel foils by means of a low-cost rotogravure printing process using environmental friendly aqueous solvents. The aim of this work is to explore new barriers preparation methods using nonvacuum and low cost techniques that could be considered by stainless steel manufacturer or companies involved in thin-film photovoltaic production.

The properties of single-layer and bilayer coatings from these nanoparticles as efficient barrier layers for thin film solar cells are discussed.

EXPERIMENTAL SECTION

Materials. Commercial stainless steel foils, AISI430 (ferritic), with 140 μm thickness were used as substrate because good adhesion for dielectric barriers had been previously reported for these foils.[22] Data corresponding to the chemical composition of S430 stainless steel substrate are presented in Table 1. The composition of the stainless steel foil consisted mainly of Fe and Cr which could diffuse into the thin film solar cell during high temperature processes and cause degradation of the solar cell efficiency. The metal foil showed a relatively high roughness (R_a) of 220 nm compared with a typical Ra of 10−15 nm for glass substrates. This elevated roughness could affect the insulation properties of the barrier layers.4

Table 1. Composition and roughness of the 140 μm-thickness steel substrate

type	C (at %)	Si (at %)	Mn (at %)	Cr (at %)	Fe (at %)	R_a (nm)
AISI430[a]	0.05	0.35	0.40	16.5	82.7	220

[a]UNS type number (Match with AISI430 ASTM designation).

For the barrier layer to block the diffusion of impurities, ceramic nanoparticles of Al_2O_3, AlN, and Si_3N_4 were chosen due to their physical properties: (i) compatible Thermal Expansion Coefficient (TEC) to that of the AISI430 foil which directly affected the film adhesion at high temperature, (ii) strong ionic interatomic bonding and nanoparticles character leading to effective impurity blocking, (iii) chemical inertness, (iv) relatively good thermal conductivity, and, (v) good electrical insulator between the metallic substrate and the monolithically interconnected solar cell required for flexible solar modules. Al_2O_3 nanoparticles were supplied by Sigma-Aldrich with particle size ranging between 20 and 50 nm. AlN nanoparticles with particle size of 40 nm were supplied by SkySpring Nanomaterials Inc. and those with particle size of 100 nm were supplied by Sigma-Aldrich. Si_3N_4 nanoparticles with particle size of 20 nm were supplied by SkySpring Nanomaterials Inc. and those with particle size of 50 nm were supplied by Sigma-Aldrich. The dispersants used for preventing nanoparticle agglomerates were poly(acrylic acid) , PEG400 and glycerin as a plasticizer, and Triton X-100 as a wetting agent. The solvent was deionized water with a conductivity of 0.055 μS cm^{-1}.

Ink formulation and Thin Film deposition. The inks were prepared from the mixture of predetermined quantities of additives (dispersant and plasticizer) with the ceramic materials (Al_2O_3, AlN, or Si_3N_4) (Scheme 1). The stability of the formulation was studied by the visual observation of sediment formation for periods up to 700 h. The name, composition and stability of the inks are summarized in Table 2.

Scheme 1. Ceramic Ink Formulation and Barrier Layer Deposition

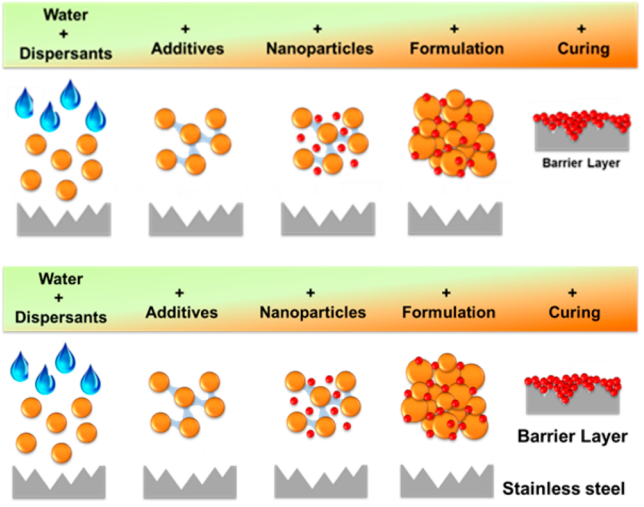

Thin films of the ceramic barriers were deposited on the substrates using a rotogravure printing process (also called doctor blade method). In this deposition approach, well-mixed slurry consisting of a suspension of ceramic particles along with other additives (such as binders, dispersants or plasticizers) was placed on a substrate before the blade. Using a constant relative movement between the blade and the substrate, the slurry spread on the substrate to form a thin sheet which resulted in a gel-layer upon drying. The blade was operated at speed up to 0.2 m s^{-1}, with a gap between the blade and the substrate of 50 μm. Finally, the thin films were sintered in air at 600 °C during 20 s.

Characterization. The ink stabilization was determined by the visual detection of sedimentation degree on time.

The thickness and roughness of the ceramic barriers were measured using a Veeco Dektac profilometer model 150. Using a 3 mg force and a 2000 μm scan length, 7 different points of the samples surface were measured to obtain an average roughness (R_a) of the surface.

To study the inks behavior at high temperature a thermal analysis using Thermogravimetry and Differential Scanning Calorimetry (TGA/DSC) was undertaken. 10−15 mg of the barrier inks were heated in air up to 600 °C at 10 °C·min^{-1} and then maintained at 600 °C during 15 min. Finally the samples were allowed to cool down to room temperature.

Table 2. Composition and Stability of the Nanoparticles Inks

inks	additives (% w/w) total	dispersant	plasticizer	ceramic materials (CM) (%w/w)	stability
			CM=Al_2O_3		
Al_2O_3–I1	3.3	1.2	2.1	2.5	unstable
Al_2O_3–I2	4.6	1.8	2.8	2.6	unstable
Al_2O_3–I3	2.5	2.2	0.3	3.0	stable
Al_2O_3–I4[a]	2.9	2.0	0.9	2.5	stable
			CM=AlN		
AlN-N1	2.0	1.8	0.2	3.0	unstable
AlN-N2	3.7	2.0	1.7	2.0	unstable
AlN-N3	4.6	2.8	1.8	2.0	stable
AlN-N4[a]	5.5	3.1	2.4	1.8	stable
			CM=Si_3N_4		
Si_3N_4–S1	5.0	1.8	3.5	2.5	unstable
Si_3N_4–S2	5.0	2.0	3.0	2.0	unstable
Si_3N_4–S3	3.9	2.1	1.8	2.0	stable
Si_3N_4–S4[a]	4.1	1.7	2.4	1.7	stable

[a]It is a mixture of particles with small and big particle size.

Fourier transform infrared spectra (FTIR-ATR) were recorded using the Spectrum 100 system from PerkinElmer in the range 4000–650 cm^{-1}.

Rheological behavior of the suspensions was investigated using a Rheometer Anton Paar Physica MCR 301. Viscosities of the ink formulations were measured at controlled shear rate (CSR mode) with a rotational speed between 1 and 100 s^{-1}.

X-ray photoelectron spectroscopy (XPS) is an ideal technique for analyzing the surface of ceramic layers and stainless steel, as it allows evaluating the diffusion process of stainless steel elements such as iron at the interface between the substrate and the ceramic layer. A PHI 5500 Multitechnique System (from Physical Electronics) with a monochromatic X-ray source Aluminum K_α line with 1486.6 eV and 350W), was used to perform the XPS measurements. The analyzed area was a circle of 0.8 mm diameter, and the selected resolution for the spectra was 187.5 eV of Pass Energy and 0.8 eV/step. In-depth measurements for composition depth profiles were obtained by sputtering the surface with an Ar+ ion source (energy of 4 keV). A profile analysis was carried out at the surface and at depths of 50, 100, 150, and 250 nm, respectively.

Ceramic layers were characterized using the ASTM D3359–09 adhesion test. This test was performed on samples with two and three ceramic layers by subjecting them to a thermal treatment at 600 °C during 45 min and 600 °C during 20 s. The metallic surface was then cut into square sections with a 20 mm side and to each of them a tape was attached. Then the tape was removed abruptly and the adhesion was assessed by determining whether the film had or not detached from the substrate.

The breakdown voltages of the ceramic barrier layers were measured to characterize the insulation properties. For this propose, a 400 nm-thick Molybdenum (Mo) layer was sputtered over the barrier-coated metal foils. The breakdown voltage was measured by connecting the Mo contacts on the barrier using a steel tip and increasing the voltage between tip and substrate until an electrical breakdown occurred.

RESULTS AND DISCUSSION

Inks Formulation. Different ink formulations were prepared by varying the relative percentage of additives and the nature of the ceramic nanoparticles. Their stabilities were analyzed by measuring the sediment as a function of time (Table 2).

The Al_2O_3 ink formulation with an additive content below 3% w/w (Al_2O_3-I_3 and Al_2O_3-I_4) showed a reasonable stability with the absence of sediment even after a period of one month. However, formulations containing over 3% w/w of additive (Al_2O_3-I_1 and Al_2O_3-I_2) presented sedimentation after 1 week. The dispersant content was increased in the Al_2O_3-I_3 and Al_2O_3-I_4 formulations and could be responsible for their absence of sedimentation. Instability of the layers of Al_2O_3 with high additive content could also be observed in the measured viscosity (Figure 1a). Stable inks, those that did not exhibit any sedimentation, showed a lower viscosity than the unstable ones (viscosity of 2.5–3 mPa s vs 11–14 mPa s). The inks must

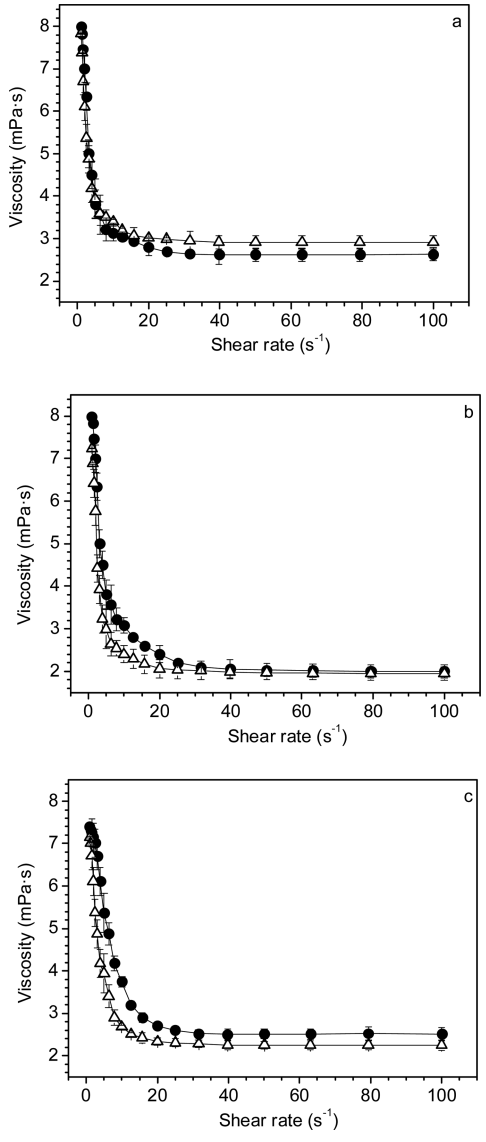

Figure 1. Viscosity curves of the stable ceramic nanoparticles inks: (a) Al_2O_3-I_3 (solid circles) and Al_2O_3-I_4 (open triangles), (b) AlN-N_3 (solid circles) and AlN-N_4 (open triangles), and (c) Si_3N_4-S_3 (solid circles) and Si_3N_4-S_4 (open triangles).

have properties of high fluidity to allow depositing thin layers. Stable ceramic inks are characterized by the non-Newtonian behavior,[23] shown in Figure 1, which is indicative of an optimal dispersion of the nanoparticles.

Moreover, AlN inks with low additive content exhibited a low stability since sediment appeared after 2 days. Ink formulations with high additive content showed good stability after one month without sedimentation (AlN-N3 and AlN-N4) because they also contained the highest content of dispersant. In contrast to inks based on Al_2O_3, AlN inks are characterized by a higher surface area which results in a higher percentage of dispersant required for the formulation stability. Therefore, both steric and electrostatic repulsion appear to be compensated by the amount of dispersant. The viscosity curves of the stable formulations show a non-Newtonian behavior.[23] As in the case of the Al_2O_3-based inks, the inks show a viscosity behavior suggesting a high stability. However, the viscosities of the AlN inks were lower than corresponding values for the Al_2O_3 inks (1.9−2 mPa s vs 2.5−3 mPa s), which may be ascribed to a higher content of plasticizer.

In the case of the Si_3N4 inks, formulations with a 5% w/w of additive (Si_3N_4-S_1 and Si_3N_4-S_2) were unstable, generating sediment content after 20 days. In these inks, a high deviation of the viscosity versus the shear stress was observed, which is indicative of their limited stabilities. The Si_3N_4-S_3 and Si_3N_4-S_4 inks, shown in Figure 1c, follow a non-Newtonian behavior, similar to that of the best Al_2O_3 and AlN formulations and with an intermediate viscosity (2−2.5 mPa s).

The evolution of the inks with temperatures up to 600 °C was analyzed by TGA/DSC. The DSC curves are characterized by an endothermic process at 105−155 °C because of dehydration followed by an exothermic behavior at 430−440 °C. The endothermic reaction was accompanied by a high weight loss, up to 95%, due to the removal of solvent.[24] In the temperature range between 160 and 600 °C, a weight reduction between 2.1 and 4.8% was observed, which may be ascribed to additive decomposition. Recovered solid powder residues after the measurement had a white color for both Al_2O_3 and Si_3N_4, and gray for AlN. These residues were analyzed using FTIR spectroscopy.

The thermal stability of the ink formulation was analyzed by comparing the FTIR spectra of the as-received ceramic materials with those of the DSC residues corresponding to the stables ceramic nanoparticles inks (Figure 2).

The absorption spectrum of the as-received Al_2O_3 nanoparticles (Figure 2a) was characterized by resolving the bands in the 650 to 1000 cm^{-1} range, which suggests the existence of AlO_4-tetrahedra and AlO_6-octahedra in their structure. No noticeable difference was observed in the IR spectra of the annealed ink formulations.

Figure 2b shows the FTIR spectrum of the AlN commercial powder which was characterized by an intense and broad band centered at 890 cm^{-1} with a shoulder at ca. 760 cm^{-1}. Li et al.[25] identified the adsorption band at 770 and 800 cm^{-1} as being due to Fröhlich modes of the nanocrystalline AlN. However, this mode can shift from one sample to other because they are quite sensitive to the crystal size and shape (i.e., Fröhlich absorption of cubical particles has a lower frequency than that of spherical particles)[26] and the dielectric constant of the medium.[27,28] In addition, the broad absorption signal could be due to the existence of a size and shape distribution. The only difference in the spectrum of the annealed ink formulation was a new absorption band at 690 cm^{-1}. This band has been

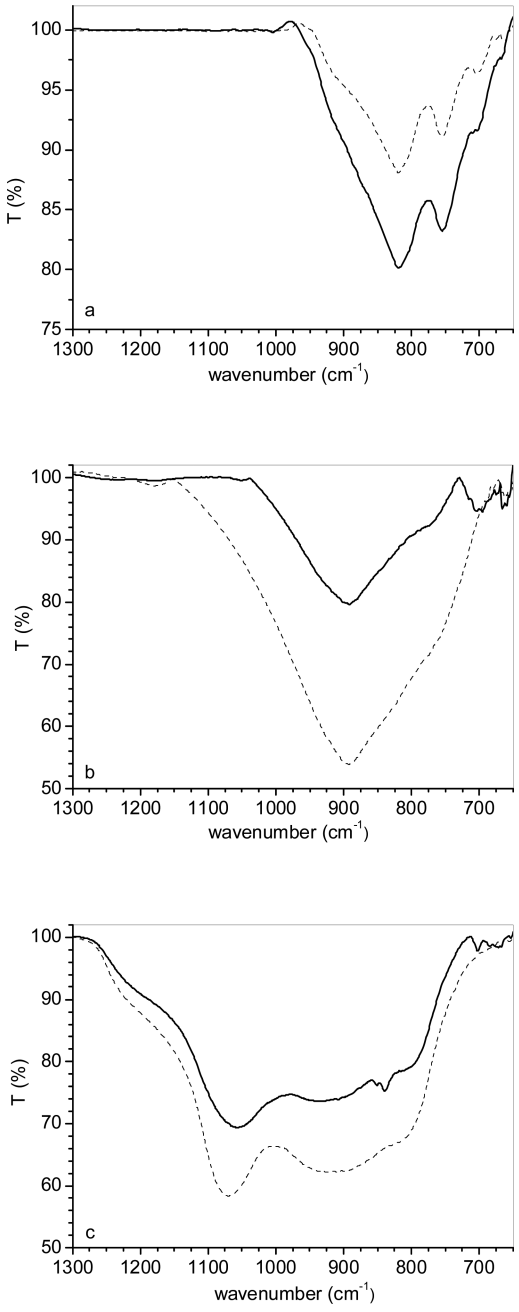

Figure 2. FT/IR spectra of as-received ceramic nanoparticles and of the DSC residues of the stable ceramic nanoparticles with homogeneous particle sizes: (a) the pristine as-received aluminum oxide nanoparticles (dash line) and Al_2O_3-I_3 (solid line), (b) the pristine as-received aluminum nitride nanoparticles (dash line) and AlN-N3 (solid line), and (c) the pristine as-received silicon nitride nanoparticles (dash line) and Si_3N_4-S_3 (solid line).

reported to belong to the Al−N band of nanostructured AlN crystals, which is close to the bulk mode at 660 cm^{-1}.[29,30] According to previous literature,[31] the existence of bulk mode can be attributed to the particle aggregation to form chainlike structure, which is favored in reduced-sized particles.

The FTIR spectra of as-received Si_3N_4 nanoparticles (Figure 2c) is characterized by a wide band in the range between 1300 and 650 cm^{-1} composed of the N−H wagging mode at ∼1150 cm^{-1} and the Si−N asymmetric stretching mode at ∼840 cm^{-1}.[32,33] The decomposition of the Si−N stretching mode

into different constituents modes (1071, 905, and 810 cm^{-1}, here) was reported for both silicon-rich[34] and stoichiometric nitride films.[35] Scardera et al.[36] attributed the shoulder in the 1000−1100 cm^{-1} range to silicon nanocrystals embedded in silicon nitride. No noticeable difference was observed in the IR spectra in the annealed ink formulation which indicated that the treatment did not induce sufficient local bonding disorder.[36]

Ceramic Barrier Deposited over a Metallic Substrate. The thickness and surface roughness as a function of the number of deposited ceramic barrier layers with homogeneous particle size are depicted in Figure 3. The thickness of the barrier increased with the number of deposited layers but this dependence was not linear. A decrease in the slope was observed on increasing the number of layers which demonstrated the influence of the substrate nature in the final thickness.[37] All ceramic barriers exhibited a decreased of the average roughness (R_a) up to a bilayer, while increasing the number of layers did not result in a further decrease of Ra. The minimum Ra measured were 109 ± 10 nm, 106 ± 14 nm, and 146 ± 5 nm for bilayers of Al_2O_3-I_3, AlN-I_3, and Si_3N_4-I_3, respectively. Thus, a relative decrease of the metal substrate roughness (220 ± 20 nm) of up to 52% was inferred. Utilizing this bilayer decreases substrate roughness resulting in improved electrical properties of the thin film cell[38] and in this respect barrier layers based on Al_2O_3 or AlN are preferable to those based on Si_3N_4.

An exploration of the influence of the particle size of the bilayer on the average roughness was performed on the ceramic barriers based on Al_2O_3 and AlN (Figure 4). A combination of small and large particle sizes reduced Ra after a second layer deposition. Therefore, the formulations with lower Ra were: AlN-N_3/AlN-N_4 (R_a = 93 ± 3 nm and thickness of 1.26 ± 0.08 μm) and Al_2O_3-I_3/Al_2O_3-I_4 (R_a = 103 ± 6 nm and thickness of 1.39 ± 0.06 μm). It is worth noting that these roughness values are quite below those measured for an Al_2O_3 barrier deposited using RF sputtering over a metal substrate.[4]

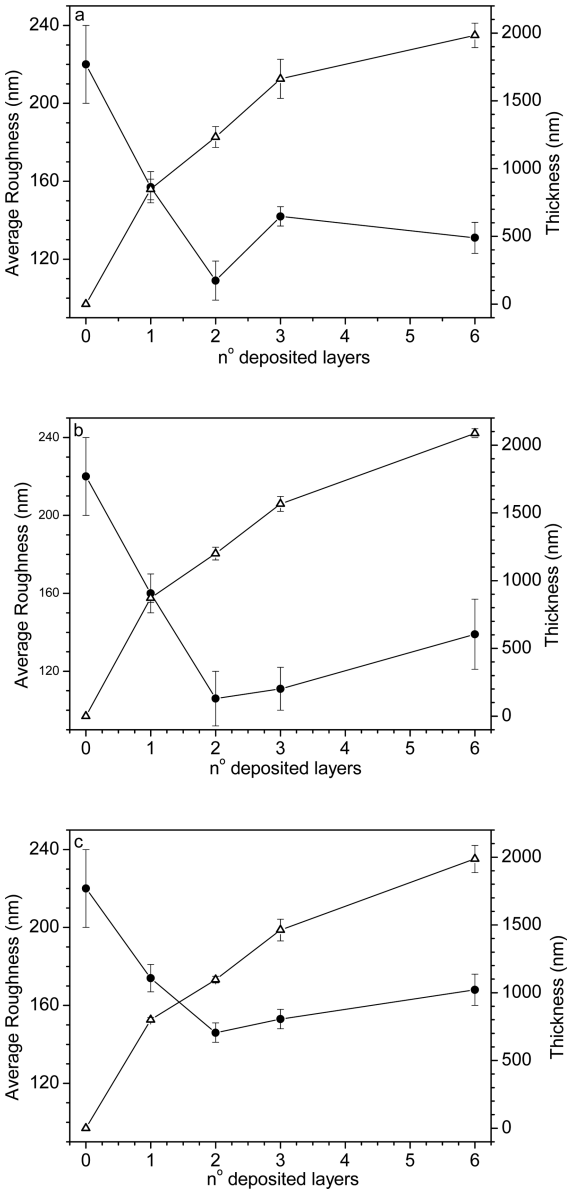

Figure 3. Average roughness (solid circles) and thickness (open triangles) of the stable ceramic barriers with homogeneous particle sizes deposited over stainless steel AISI430: (a) Al_2O_3-I_3, (b) AlN-N_3, and,(c) Si_3N_4-S_3.

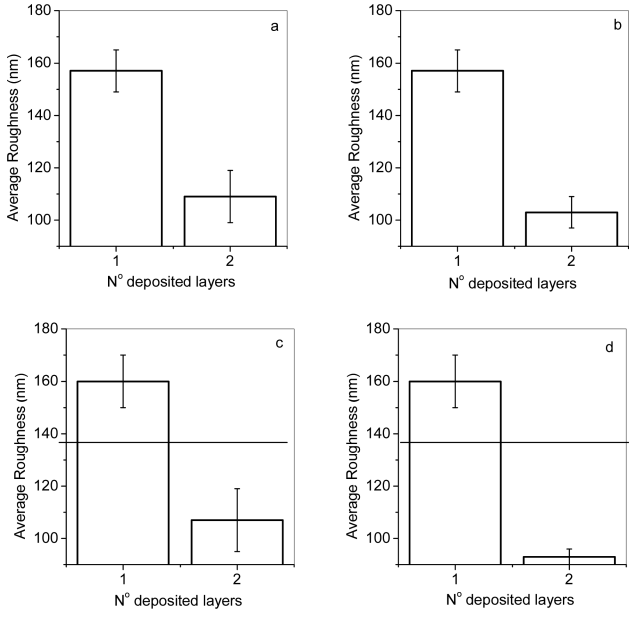

Figure 4. Average roughness and thickness of a bilayer ceramic barrier as a function of the nature of the second layer: (a) bilayer Al_2O_3-I_3/Al_2O_3-I_3, (b) bilayer Al_2O_3-I_3/Al_2O_3-I_4, (c) bilayer AlN-N_3/AlN-N_3, and (d) bilayer AlN-N_3/AlN-N_4.

Both thin barrier layers, Al_2O_3 and AlN, displayed a good adhesion to the metal substrate even after thermal treatments at 600 °C during 45 min. Additionally, no film cracking was observed in the barrier layers after doctor blade deposition. The absence of cracks or exfoliation in annealed samples also suggests a high-quality barrier obtained using the previously described procedure.

The ability of both ceramic bilayer barriers (AlN-N_3/AlN-N_4, and Al_2O_3-I_3/Al_2O_3-I_4) to both reduce the diffusion of impurities from the metal substrate into the solar cell and provide electrical insulation between the metal substrate and the device were explored.

The diffusion of metals atoms through the Mo back contact into the photovoltaic active layers can decrease device efficiency for thin film solar cells fabricated over flexible metal foils. The diffusion of metals atoms can cause enhancement of

recombination processes at these metal impurities resulting in a decrease in the collection of carriers at the electrodes. The deposition temperatures required to deposit both the absorber layer and the front contact (typically above 550 °C) can result in metal impurity diffusion and therefore diffusion of Fe atoms through the barriers was investigated using XPS. The intensity of both Fe $2p_3$ and Fe $2p_1$ XPS signals of a bilayer of AlN-N_3/AlN-N_4 and a bilayer of Al_2O_3-I_3/Al_2O_3-I_4 deposited over AISI430 stainless steel and heated at 600 °C during 45 min are shown in Figure 5. For both ceramic barriers, the intensity of

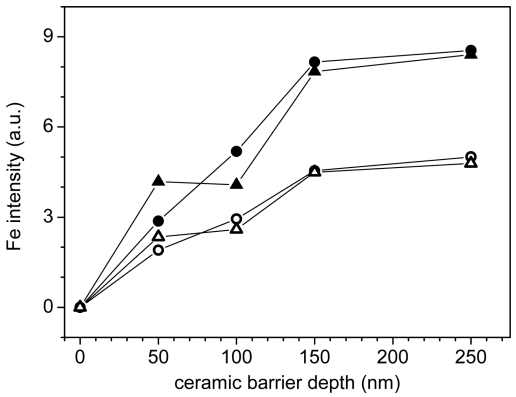

Figure 5. Intensity profile for the Fe $2p_3$ (solid symbols) and Fe $2p_1$ (open symbols) XPS signals corresponding to AlN-N3/AlN-N4 bilayer (circles) and Al_2O_3-I_3/Al_2O_3-I_4 bilayer (triangles) deposited over AISI430 stainless steel and heated at 600 °C during 45 min.

the signals decreases to zero at the surface, which suggests that a barrier of both materials with a thickness of roughly 1.3 μm is sufficient to avoid metal-impurity diffusion through the Mo back contact layer.

Finally, the breakdown voltages were measured for both bilayers barriers (AlN-N_3/AlN-N_4 and Al_2O_3-I_3/Al_2O_3-I_4 and are shown in Figure 6. The values were 32 V for the 1.39 μm-

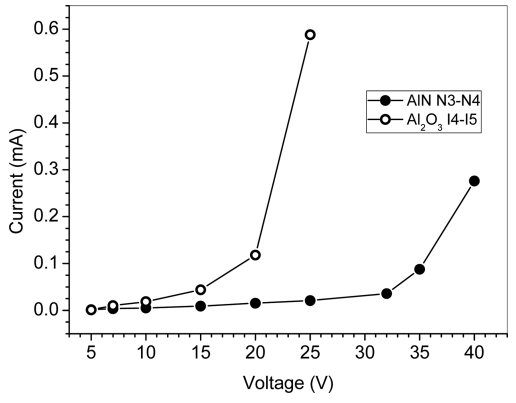

Figure 6. Dielectric breakdown curves corresponding to AlN-N_3/AlN-N_4 bilayer (solid line) and Al_2O_3-I_3/Al_2O_3-I_4 bilayer (dash line) deposited over AISI430 stainless steel and covered by a molybdenum layer.

thick AlN-N3/AlN-N4 barriers and 20 V for the 1.26 μm-thick Al_2O_3-I_3/Al_2O_3-I_4 structures, respectively. These values are similar to those reported for 1 μm-thick RF-sputtered Al_2O_3 barriers, with the advantage that the present work uses low-cost high throughput fabrication methods alone.[4] Low breakdown voltages suggest a poor electrical insulation behavior of the barriers.

CONCLUSIONS

Ceramic inks using water as solvent have been formulated and the conditions of formulation to ensure stability and an adequate flow have been determined.

The optimum number of layers is a bilayer which is able to decrease the roughness. In this sense, the best formulations were a bilayer of Al_2O_3-I_3/Al_2O_3-I_4 or AlN-N_3/AlN-N_4, which also prevented the diffusion of metals through the dielectric barrier. Among them, the bilayer of AlN-N_3/AlN-N_4 exhibited the best insulation properties.

Moreover, an easily scalable deposition technique has been proposed. It has some advantages that ensure their acceptance at industrial scale: low CAPEX, high throughput, nonexpensive raw materials, and high exploitation efficiency compared to vacuum techniques ones. The chemical solutions employed are REACH rules compatible: nontoxic elements are used and noncontaminant residues are generated.

AUTHOR INFORMATION

Corresponding Authors

* E-mail: josemaria.delgado@solar.abengoa.com.

*E-mail: alba@icmse.csic.es.

Notes

The authors declare no competing financial interest.

ACKNOWLEDGMENTS

We good like to acknowledge Prof. Francisco Villuendas for fruitful discussions. We thank also to F.J Castaño for fruitful discussions and manuscript proof reading.

REFERENCES

(1) Contreras, M. A.; Romero, M. J.; Noufi, R. Characterization of Cu(In,Ga)Se_2 Materials Used in Record Performance Solar Cells. *Thin Solid Films* **2006**, *511*, 51−54.

(2) Green, M. A.; Emery, K.; Hishikawa, Y.; Wart, W. Solar Cell Efficiency Tables (version 37). *Prog. Photovoltaics* **2011**, *19*, 84−92.

(3) Schultz, O.; Glunz, G. W.; Willeke, G. P. Multicrystalline Silicon Solar Cells Exceeding 20% Efficiency. *Prog. Photovoltaics* **2004**, *12*, 553−558.

(4) Hertz, K.; Kessler, F.; Wächter, R.; Powalla, M.; Scneider, J.; Schulz, A.; Schumacher, U. Dielectric Barriers for Flexible CIGS Solar Modules. *Thin Solid Films* **2002**, *403−404*, 384−389.

(5) Contreras, M.; Egas, B.; Ramanathan, K.; Hiltner, J.; Hasson, F.; Noufi, R. Progress Toward 20% Efficiency in Cu(In,Ga)Se2 Polycrystalline Thin-film Solar Cells. *Prog. Photovoltaics* **1999**, *7*, 311−316.

(6) Basol, B. M.; Kapur, V. K.; Leidholm, C. R.; Halani, A. Flexible and Light Weight Copper Indium Diselenide Solar Cells on Polyimide Substrates. *Sol. Energy Mater. Sol. Cells* **1996**, *43*, 93−98.

(7) Tiwari, A. N.; Krejci, M.; Haug, F. J.; Zogg, H. 12.8% Efficiency Cu(In,Ga)Se_2 Solar Cell on a Flexible Polymer Sheet. *Prog. Photovoltics* **1999**, *7*, 393−397.

(8) Bermaud, D.; Rudmann, D.; Kaelin, M.; Ermits, K.; Bilger, G.; Dobeli, M.; Zogg, H.; Tiwari, A. N. Flexible Cu(In,Ga)Se2 on Al Foils and the Effects of Al During Chemical Bath Deposition. *Thin Solid Films* **2007**, *515*, 5857−5861.

(9) Ishizuka, S.; Yamada, A.; Matsubara, K.; Fons, P.; Sakurai, K.; Niki, S. Alkali Incorporation Control in Cu(In,Ga)Se_2 Thin Flms Using Silicate Thin Layers and Applications in Enhancing Flexible Solar Cell Efficiency. *Appl. Phys. Lett.* **2008**, *93*, 1241051−1241053.

(10) Ishizuka, S.; Yamada, A.; Islam, M. M.; Shibata, H.; Fons, P.; Sakurai, T.; Akimoto, K.; Niki, S. Na-induced Variations in the

Structural, Optical, and Electrical Properties of Cu(In,Ga)Se2 Thin Flms. *J. Appl. Phys.* **2009**, *106*, 0349081−0349086.
(11) Yagioka, T.; Nakada, T. Cd-Free Flexible Cu(In,Ga)Se2 Thin Film Solar Cells with ZnS(O,OH) Buffer Layers on Ti Foils. *Appl. Phys. Express* **2009**, *2*, 0722011−0722016.
(12) Kessler, F.; Rudmann, D. Technological Aspects of Flexible CIGS Solar Cells and Modules. *S. Energy* **2004**, *77*, 685−695.
(13) Chirilă, A.; Buecheler, S.; Pianezzi, F.; Bloesch, P.; Gretener, C.; Uhl, A.; Fella, C.; Kranz, L.; Perrenound, J.; Seyrling, S.; Verma, R.; Nishiwaki, S.; Romanyuk, Y. E.; Bilger, G.; Tiwari, A. N. Highly Efficient Cu(In,Ga)Se2 Solar Cells Grown on Flexible Polymer Films. *Nat. Mater.* **2011**, *10*, 857−861.
(14) Kawakita, S.; Imaizumi, M.; Sumita, T.; Kushiya, K.; Ohshima, T.; Yamaguchi, M. Super Radiation Tolerance of CIGS Solar Cells Demonstrated in Space by MSD-1 Satellite. In *Proceedings of the 3rd World Conference Photovoltaic Energy Conversion*; Osaka, May 11−18, 2003 ; IEEE: Piscataway, NJ, 2003; pp 693−696.
(15) Otte, K.; Makhova, I.; Braun, A.; Konovalov, I. Flexible Cu(In,Ga)Se2 Thin-Film Solar Cells for Space Application. *Thin Solid Films* **2006**, *511−512*, 613−622.
(16) Jackson, P.; Hariskos, D.; Lotter, E.; Paetel, S.; Wuerz, R.; Menner, R.; Wischmann, W.; Powalla, M. New World Record Efficiency for Cu(In,Ga)Se_2 Thin-Film Solar Cells Beyond 20%. *Prog. Photovoltaics* **2011**, *19*, 894−897.
(17) Guillen, C.; Martinez, M. A.; Maffiotte, C.; Herrero, J. Chemistry of CdS/$CuInSe_2$ Structures as Controlled by the CdS Deposition Bath. *J. Electrochem. Soc.* **2001**, *11*, G602−G606.
(18) Kessler, F.; Hermann, D.; Powalla, M. Approaches to Flexible CIGS Thin-Film Solar Cells. *Thin Solid Films* **2001**, *480−481*, 491−498.
(19) Guillemoles, J.; Kronik, L.; Cahen, D.; Rau, U.; Jasenek, A.; Schock, H. W. Stability Issues of Cu(Ga,In)Se-based Solar Cells. *J. Phys. Chem. B* **2000**, *104*, 4849−4862.
(20) Bae, D. W.; Gho, J.; Shin, M.; Kwon, S. Effect of Zinc Addition on Properties of Cadmium Sulfide Layer and Performance of Cu(In,Ga)Se2 Solar Cells. *Thin Solid Films* **2013**, *535*, 162−165.
(21) Herz, K.; Eicker, A.; Kessler, F.; Wächter, R.; Powalla, M. Diffusion Barriers for CIGS Solar Cells on Metallic Substrates. *Thin Solid Films* **2003**, *431−432*, 392−397.
(22) Thongkham, W.; Pankiew, A.; Yoodee, K.; Chatraphorn, S. Enhancing Efficiency of Cu(In,Ga)Se_2 Solar Cells on Flexible Stainless Steel Foils Using NaF Co-evaporation. *S. Energy* **2013**, *92*, 189−195.
(23) Bouldin, M.; Kulicke, W.-M; Kehler, H. Prediction of the Non-Newtonian Viscosity and Shear Stability of Polymer Solutions. *Colloid Polym. Sci.* **1988**, *266*, 793−805.
(24) Datta, S.; Keller, K.; Schulz, D. L.; Webster, D. C. Conductive Adhesives From Low-VOC Silver Inks for Advanced Microelectronics Applications. *IEEE Trans. Compon., Packag., Manuf. Technol.* **2011**, *1*, 69−75.
(25) Li, H. D.; Zou, G. T.; Wang, H.; Yang, H. B.; Li, D. M.; Yu, S.; Wu, Y.; Meng, Z. F. Synthesis and Infrared Study of Nanosized Aluminum Nitride Powders Prepared by Direct Current Arc Plasma. *J. Phys. Chem. B* **1998**, *102*, 8692−8695.
(26) LuXon, J. T.; Montgomery, D. J.; Summitt, R. Effect of Particle Size and Shape on Infrared Absorption of Magnesium Oxide Powders. *Phys. Rev.* **1969**, *188*, 1345−&.
(27) Yamamoto, K.; Tran, C. D.; Shimizu, H.; Abe, K. Optical Surface Phonon Modes in ZnO Small Crystals. *J. Phys. Soc. Jpn.* **1977**, *42*, 587−590.
(28) Ruppin, R.; Nahum, J. Phonon-plasmon Modes in Small GaN Crystals. *J. Phys. Chem. Solids* **1974**, *35*, 1311−1315.
(29) Chen, X.; Gonsalves, K. E. Synthesis and Properties of an Aluminum Nitride/Polyimide Nanocomposite Prepared by a Non-aqueous Suspension Process. *J. Mater. Res.* **1997**, *12*, 1274−1286.
(30) Gonsalves, K. E.; Jin, S.; Baraton, M. Microparticles of Functionalized Polylactide Copolymers. *Mater. Res. Soc. Symp. Proc.* **1998**, *501*, 233−238.
(31) Hayshi, S.; Nakamori, N.; Hirono, J.; Kanamori, H. Infrared Study of Surface Vibration Modes in MgO Small Cubes. *J. Phys. Soc. Jpn.* **1977**, *43*, 2006−2012.
(32) Lucovsky, G.; Yang, J.; Chao, S. S.; Tyler, J. E.; Czubatyj, W. Nitrogen-bonding Environments in Glow-discharge Deposited a-Si:H Films. *Phys. Rev. B* **1983**, *28*, 3234−3240.
(33) Tsu, D. V.; Lucovsky, G.; Mantini, M. J. Local Atomic Structure in Thin Films of Silicon Nitride and Silicon Diimide Produced by Remote Plasma-enhanced Chemical-vapor Deposition. *Phys. Rev. B* **1986**, *33*, 7069−7076.
(34) Hasegawa, S.; Ambutsu, H.; Kurata, Y. Connection Between Si−N and Si−H Vibrational Properties in Amorphous SiNx: H Films. *Philos. Mag. B* **1989**, *59*, 365−375.
(35) Bustarret, E.; Besouda, M.; Habrard, M. C.; Bruyêre, J.; Poulin, S.; Gujrathi, S. C. Configurational Statistics in a-Si, NyH, Alloys: A Quantitative Bonding Analysis. *Phys. Rev. B* **1988**, *38*, 8171−8184.
(36) Scardera, G.; Puzzer, T.; Conibeer, G.; Green, M. A. Fourier Transform Infrared Spectroscopy of Annealed Silicon-rich Silicon Nitride Thin Films. *J. Appl. Phys.* **2008**, *104*, 1043101−1043107.
(37) Asgari, H.; Ashrafizadeh, F.; Toroghinejad, M. R. Influence of Steel Substrate Grain Size on Phase Layers Growth Kinetics and Thickness of Zinc Hot Dipped Steel Sheets. *Ironmaking Steelmaking* **2009**, *36*, 145−148.
(38) Amouzou, D.; Guaino, P.; Fourdrineier, L.; Richir, J. B.; Maseri, F.; Sporken, R. Dielectric and Diffusion Barrier Multilayer for Cu(In,Ga)Se2 Solar Cells Integration on Stainless Steel Sheet. *Thin Solid Films* **2013**, *542*, 270−275.